nature nanotechnology

LETTERS

PUBLISHED ONLINE: 13 FEBRUARY 2011 | DOI: 10.1038/NNANO.2011.3

Gate-controlled guiding of electrons in graphene

J. R. Williams[1,3†], Tony Low[2], M. S. Lundstrom[2] and C. M. Marcus[3*]

Ballistic semiconductor structures have allowed the realization of optics-like phenomena in electronic systems, including the magnetic focusing[1] and electrostatic lensing[2] of electrons. An extension that appears unique to graphene is to use both n and p carrier types to create electronic analogues of optical devices with both positive and negative indices of refraction[3]. Here, we use the gate-controlled density of both p and n carrier types in graphene to demonstrate the electronic analogue of fibre-optic guiding[4–8]. Two basic effects are investigated: bipolar p–n junction guiding, based on the principle of angle-selective transmission through the interface between the graphene and the p–n junction; and unipolar fibre-optic guiding, using total internal reflection controlled by carrier density. We also demonstrate modulation of the guiding efficiency through gating, and comparison of these data with numerical simulations indicates that guiding performance is limited by the roughness of the interface. The development of p–n and fibre-optic guiding in graphene may lead to electrically reconfigurable wiring in high-mobility devices.

Graphene is a single-layer hexagonal lattice of carbon atoms with a gapless, linear dispersion that leads to novel electronic properties[9,10]. Carrier type and density can be controlled via gates, creating high-mobility, bipolar graphene electronics[11]. Electronic transport across an interface of holes (p) and electrons (n) (a p–n junction) has been studied experimentally using a combination of top/bottom electrostatic gates to create p and n regions[12–14], and is now well understood theoretically[15–19].

An intriguing possibility is to use both n and p carrier types in bipolar graphene structures to create electronic analogues of optical devices with both positive and negative indices of refraction. For example, a symmetrically biased p–n junction has been shown theoretically to create a negative refractive index medium analogous to a Veselago lens[3]. Such a device is not possible using conventional two-dimensional electron gas (2DEG) systems, and demonstrates a unique feature of a Dirac-like band structure in conjunction with the ability to electrostatically tune between n and p carrier types. There is considerable theoretical interest in using the Dirac-like properties of graphene to create novel optical devices in graphene[4–8,20–24], but experiments on these systems have not yet been reported.

In this Letter, we demonstrate experimentally and numerically the graphene analogue of a well-known optical device, the fibre optic. Three regimes of current guiding are identified in the experiment and simulations: (i) p–n junction guiding, based on the principle of angle-selective transmission, (ii) the graphene fibre-optic analogue, using total internal reflection, and (iii) a mixture of the two effects. A metric of the guiding efficiency is predicted in all three regimes. By varying the external parameters of gate voltage and magnetic field, guiding efficiencies in each regime are extracted from experiment, and trends in the parameters are observed and compared to numerical simulations.

Photons and electrons exhibit analogous wave phenomena, reflected in the similarity of the Helmholtz equation describing electromagnetic wave propagation and the Schrödinger equations describing propagation for electrons[25,26]. In graphene, the Fermi energy (ε) plays the role of the index of refraction in an optical medium[3–8], with the important feature that ε can be modified via electrostatic gates. Note that the dependence of the effective index of refraction on density and gate voltage in graphene differs from the dependence in conventional 2DEGs. In graphene, the wave number, and hence the effective index, is proportional to ε. In conventional 2DEGs, the wave number and effective index scale as $\varepsilon^{1/2}$ (ref. 2). More significantly, for graphene, ε can either be positive (for electrons) or negative (for holes).

For the device shown schematically in Fig. 1a, the effective index of refraction under the top gate (Region 1), ε_1, is controlled by the combined voltages on the top gate, V_{TG}, and backgate, V_{BG}, while the

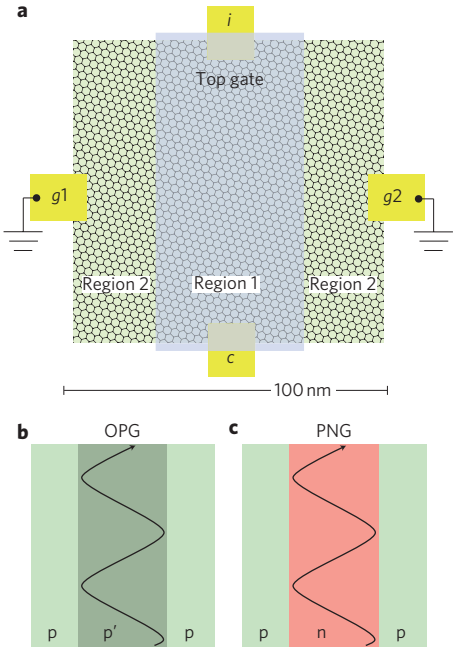

Figure 1 | Schematics of the device and guiding in unipolar and bipolar regimes. a, Schematic of a top-gated electron guiding device with four contacts (*i*, *c*, *g*1 and *g*2) used to measure resistances R_{ii}, R^f_{ii} and R^f_{ic}. Voltages on the top gate, V_{TG}, and the back gate, V_{BG} (not shown) independently control carrier densities (including sign), which serve as effective indices of refraction. Graphene lattice orientation is schematic and is not controlled. **b**, OPG is based on reflection above a critical angle when the density in the channel (under the top gate) is higher than outside the channel (controlled by the back gate), similar to the operation of a fibre optic. **c**, Alternatively, PNG is based on exponentially suppressed transmission through a p–n interface at oblique angles of incidence.

[1]School of Engineering and Applied Sciences, Harvard University, Cambridge, Massachusetts 02138, USA, [2]School of Electrical & Computer Engineering, Purdue University, West Lafayette, Indiana 47906, USA, [3]Department of Physics, Harvard University, Cambridge, Massachusetts 02138, USA; [†]Present address: Department of Physics, Stanford University, Stanford, California 94305, USA. *e-mail: marcus@harvard.edu

effective index of refraction outside the top-gated region (Region 2), ε_2, is controlled only by V_{BG}. When $|\varepsilon_1| > |\varepsilon_2|$, the device operates as an electronic fibre optic with critical angle $\theta_c = \sin^{-1}(|\varepsilon_2/\varepsilon_1|)$. This effect, termed optical guiding (OPG), is shown schematically in Fig. 1b. Modes propagating with $\theta \geq \theta_c$ will be totally internally reflected and therefore travel down the channel without leaking out of the fibre.

Transmission across a graphene p–n interface decreases exponentially with angle from the interface normal[15]. Therefore, at grazing incidence, nearly all carriers impinging on the p–n interface are reflected, which leads to guiding of all but a small number of carriers. This guiding mechanism is termed p–n guiding (PNG) and is shown schematically in Fig. 1c. Depending on the values of V_{TG} and V_{BG}, the mechanism responsible for guiding will be either OPG, PNG or a combination of the two (OPG/PNG). The carrier-density locations of these three regions are shown as a function of the density under the top gate (n_1) and outside the top gate (n_2) in Fig. 2a. For unipolar devices (no p–n junctions, shaded blue), only OPG is present. For bipolar devices (shaded red), both PNG and OPG/PNG can occur. OPG occurs if $|\varepsilon_1| > |\varepsilon_2|$; PNG occurs if $\varepsilon_1 \times \varepsilon_2 < 0$; OPG/PNG occurs if both conditions are satisfied.

Quantum transport simulations are used to extract guiding efficiency as a function of gate voltage (see Supplementary Information for numerical methods). The simulated device (Fig. 1a) has four contacts, i (injector), c (collector), $g1$ and $g2$ (electrical ground 1, 2) (Fig. 1a). Guiding efficiency is defined as the fraction of current collected at c due to injection from i, $\Omega = \mathcal{T}_{ic}/\mathcal{T}_{ii}$, where $\mathcal{T}_{mn}$ is the transmission probability from contact m to n, and $\mathcal{T}_{ii} = \mathcal{T}_{ic} + \mathcal{T}_{ig1} + \mathcal{T}_{ig2}$. Note that Ω is finite even for equal indices of refraction in Regions 1 and 2, because $\mathcal{T}_{ic}$ is non-zero when $\varepsilon_1 = \varepsilon_2$ (that is, a uniformly biased graphene sheet). We therefore define γ as the difference between Ω and its value for equal indices,

$$\gamma(\varepsilon_1, \varepsilon_2) = \Omega(\varepsilon_1, \varepsilon_2) - \Omega(\varepsilon_1, \varepsilon_1) \quad (1)$$

The parameter $\gamma(\varepsilon_1, \varepsilon_2)$ then serves as an effective measure of the guiding efficiency due to unequal indices of refraction for the graphene channel, independent of the source of guiding. The condition $\Omega(\varepsilon_1, \varepsilon_1) = \Omega(-\varepsilon_1, -\varepsilon_1)$ follows from particle–hole symmetry. We take Fermi energy to be equivalent to the effective index of refraction, and so equate ε_1 and ε_2 with Fermi energies in Regions 1 and 2.

Simulations for a 100 nm × 100 nm device (matching the experimental geometry) in the OPG, PNG and OPG/PNG regimes (Fig. 2b–d) yield guiding efficiencies $\Omega(-0.3\text{ eV}, -0.2\text{ eV}) = 0.58$ for OPG, $\Omega(0.2\text{ eV}, -0.2\text{ eV}) = 0.18$ for PNG, and $\Omega(0.3\text{ eV}, -0.2\text{ eV}) = 0.29$ for OPG/PNG. Using $\Omega(0.3\text{ eV}, 0.3\text{ eV}) = 0.05$ (Fig. 2b,d) and $\Omega(0.2\text{ eV}, 0.2\text{ eV}) = 0.15$ (Fig. 2c) gives $\gamma = 0.53$ for OPG, $\gamma = 0.03$ for PNG and $\gamma = 0.24$ for OPG/PNG. To obtain these values, simulations assumed a root-mean-square interface roughness of 4 nm in the p–n case and no roughness in the p–p interface. Adding roughness is neccessary to obtain the qualitative trend observed experimentally, $\Omega^{OPG} > \Omega^{OPG/PNG} > \Omega^{PNG}$; without interface roughness for the p–n case, numerics gave $\Omega^{OPG} \leq \Omega^{OPG/PNG}$. The larger roughness in the p–n regime presumably reflects the poor screening of disorder at the zero-density p–n junction[27] and is consistent with the theoretical observation that large-angle scattering modes are deteriorated by disorder[28]. For a p–p interface, a larger Ω than experiments is obtained when assuming an ideal p–p interface. It is therefore necessary to also add some roughness to the p–p interface to obtain quantitative agreement with experiment, as seen in Fig. 3.

We next discuss the experimental realization of electron guiding. Devices were made by mechanical exfoliation of highly oriented pyrolytic graphite. Metallic contacts (i, c, $g1$ and $g2$) were patterned with electron-beam lithography (Fig. 1a), and the size of the device was reduced to 100 nm × 100 nm using an O_2/Ar_2 plasma etch, giving a device of dimensions comparable to its mean free path, determined

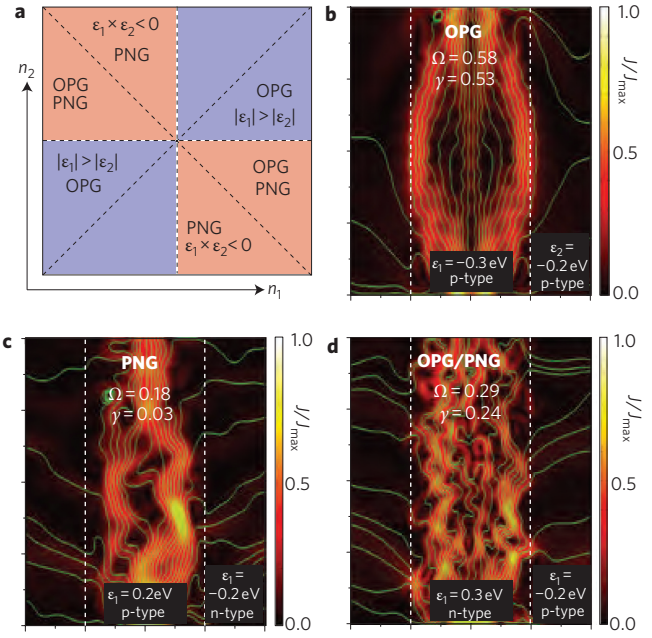

Figure 2 | Simulated optical and p–n guiding in gated graphene. a, Guiding regimes (OPG (blue), PNG and OPG/PNG (pink)) as a function of density under the top gate (n_1) and outside the top gate (n_2). The midpoint of the diagram is zero density in Regions 1 and 2. **b–d**, Simulations of the current density J in the three regimes for fixed effective index of refractions ε_1 and ε_2. The x-and y-axes represent the 100 nm × 100 nm size scale of the device. The guiding efficiency is $\gamma = 0.53$, 0.03 and 0.24 ($\Omega = 0.58$, 0.18 and 0.29) in the OPG, PNG and OPG/PNG regimes, respectively. Green lines in **b–d** are lines of constant current density.

by transport. A functionalized, top-gate oxide was grown[13] and a top-gate electrode patterned using electron-beam lithography. Differential resistance $R = \mathrm{d}I/\mathrm{d}V$ was measured using a standard lock-in technique at a temperature of $T = 30$ K. Relatively high temperature and large densities were used to suppress Coloumb blockade fluctuations of the resistance present in the small device at low temperatures and densities. The field-effect, Drude mean free path $\ell_{mfp} = h/e^2 \cdot \sigma/k_F$, where $k_F = \sqrt{\pi |n_s|}$, for micrometre-sized graphene sheets is routinely found to be $\gtrsim$100 nm away from the charge neutrality point. Here, however, it is difficult to estimate ℓ_{mfp} in these sub-micrometre devices, as the charging energy will create deviations from the simple Drude model. Extracting ℓ_{mfp} from a four-terminal measurement $R(V_{TG})$ yields ~70 nm. Given the limitations of the Drude ℓ_{mfp}, the device is at the very least in the quasi-ballistic regime.

Experimental guiding efficiency $\Omega_{exp} = \mathcal{T}_{ic}/\mathcal{T}_{ii}$ is determined from transport measurements. Transmission $\mathcal{T}_{ii}$ is obtained in a 'channel' geometry, with current I_i applied to i, and c, $g1$ and $g2$ grounded, from the resistance $R_{ii} = V_i/I_i$,

$$\mathcal{T}_{ii} \approx \frac{h/2e^2}{R_{ii}} \quad (2)$$

Transmission $\mathcal{T}_{ic}$ is measured in a 'focusing' geometry[1], with current I_i applied to i, voltage measured at c, and $g1$ and $g2$ grounded. Using this geometry, two resistances are measured by monitoring the voltages at contacts i and c: $R^f_{ii} = V_i/I_i$ and $R^f_{ic} = V_c/I_i$. A calculation of Ω_{exp} could be made by taking the ratio of these two resistances; however, the symmetry $\mathcal{T}_{ic} = \mathcal{T}_{ci}$ and $\mathcal{T}_{ii} = \mathcal{T}_{cc}$ may not hold in real devices. Accounting for deviation from the above idealities, we average Ω_{exp} over the two configurations $\Omega_{exp} = \mathcal{T}_{ci}/\mathcal{T}_{ii}$ and $\Omega_{exp} = \mathcal{T}_{ic}/\mathcal{T}_{cc}$ to obtain a value for guiding in

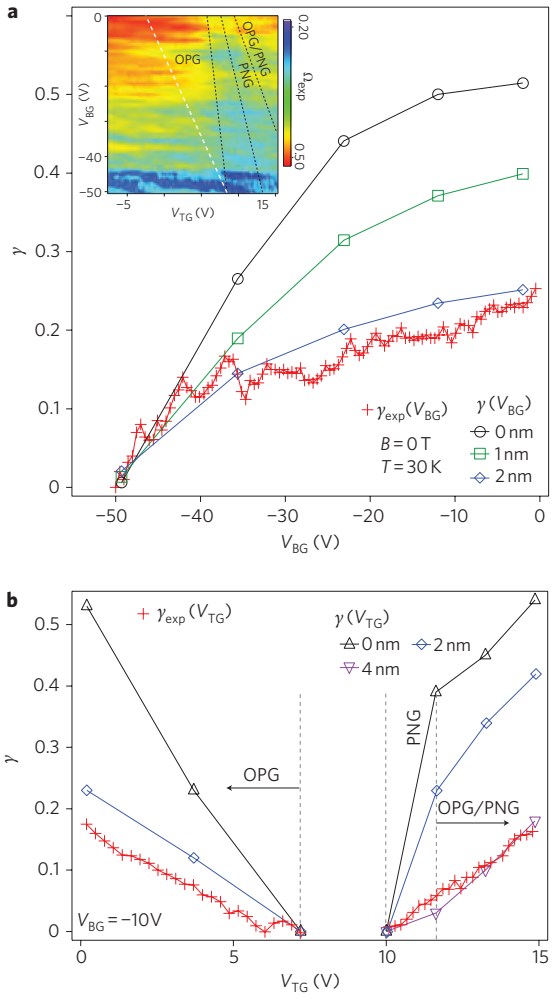

Figure 3 | Effects of gating and disorder on guiding efficiency a. Inset: experimental guiding efficiency Ω_{exp} (colour scale) as a function of top-gate voltage, V_{TG}, and back-gate voltage, V_{BG}, extracted from the resistances R_{ii}, R^f_{ii} and R^f_{ic}, with three guiding regimes indicated (black dashed lines). Cut line (white dashed line) through the OPG regime indicates where experimental and numerical guiding efficiencies are compared in the main figure. Main panel: experimental guiding efficiency γ_{exp} along constant Fermi energy (effective index of refraction) in Region 1, $\varepsilon_1 = 0.3$ eV. The value of γ_{exp} rises from 0 at $V_{BG} = -50$ V (the point where the density is a constant in the device) to ~0.20 at $V_{BG} = 0$ V. Numerical guiding efficiencies are plotted for interface roughnesses of 0 (black circles), 1 nm (green squares) and 2 nm (blue diamonds). **b**, γ_{exp} extracted along $V_{BG} = -10$ V (red crosses) shows the extracted guiding in the OPG, PNG and OPG/PNG regimes along with γ from simulation with disorder of 0 (black) and 2 nm (blue) in the OPG regime and 0 (black), 2 (blue) and 4 nm (purple) in the PNG and OPG/PNG regimes. Good agreement between experiment is observed for 2 nm in the OPG regime and 4 nm for the PNG and OPG/PNG regimes.

terms of resistances R^f_{ii} and R^f_{ic} (see Supplementary Information),

$$\Omega_{exp} \approx \frac{1}{2}\left(\frac{R^f_{ii} - R_{ii}}{R^f_{ic}} + \frac{R^f_{ic}}{R^f_{ii}}\right) \quad (3)$$

where the two terms in equation (3) are $\mathcal{T}_{ci}/\mathcal{T}_{cc}$ and $\mathcal{T}_{ic}/\mathcal{T}_{ii}$ respectively. Ideally, the symmetry of the device would entail $\mathcal{T}_{ci} = \mathcal{T}_{ic}$ and $\mathcal{T}_{ii} = \mathcal{T}_{cc}$, and equation (3) would reduce to $\Omega = \mathcal{T}_{ic}/\mathcal{T}_{ii}$. However, this will not be the case in typical experimental conditions due to disorder and contact misalignment. A quantitative estimation of the experimental guiding efficiency is obtained by taking the average of $\Omega_{exp} = \mathcal{T}_{ci}/\mathcal{T}_{ii}$ and $\Omega_{exp} = \mathcal{T}_{ic}/\mathcal{T}_{cc}$, producing equation (3). Because $0 < \Omega_{exp} < 1$, one also has the inequalities $R^f_{ii} - R_{ii} > 0$, $R^f_{ii} - R_{ii} < R^f_{ic}$ and $R^f_{ic} < R^f_{ii}$, in agreement with experiment (see Supplementary Information).

Values for Ω_{exp} as a function of top- and back-gate voltages, extracted R_{ii}, R^f_{ii} and R^f_{ic}, are shown in the inset of Fig. 3, together with boundaries of the guiding regimes based on the boundaries in Fig. 2a. Ω_{exp} is maximal in the OPG and OPG/PNG regimes, and follows the pattern $\Omega^{OPG}_{exp} > \Omega^{OPG/PNG}_{exp} > \Omega^{PNG}_{exp}$.

Experimental and numerical results for guiding efficiency are compared in the OPG regime, where guiding is most efficient, along a cut at constant density (Fermi energy $\varepsilon_1 \approx 0.3$ eV) in Region 1, indicated by the white dashed line in the inset of Fig. 3a. Experimental guiding efficiency γ_{exp} along this cut is obtained from Ω_{exp} by subtracting $\Omega_{exp}(0.3\text{ eV}, 0.3\text{ eV}) = 0.26$. Figure 3 shows γ_{exp} as a function of V_{BG} in the OPG regime, together with numerical results for $\varepsilon_1 = 0.3$ eV with numerical interface roughnesses of 0, 1 and 2 nm. Numerical values of γ were computed from Ω using $\Omega(0.3\text{ eV}, 0.3\text{ eV}) = 0.05$. For all values of interface roughness, γ increases with increasing V_{BG} (or decreasing $|\varepsilon_2|$), and good quantitative agreement with experiment is found for a roughness of 2 nm. The dependence of γ on V_{BG} can be understood by analogy with optical fibre, where decreasing the refractive index in the fibre cladding $|\varepsilon_2|$ leads to a smaller critical angle. The inset of Fig. 3 shows that the trend of increasing Ω_{exp} with back-gate voltage is more prominent in the OPG regime than in the PNG regime. This is consistent with expectation, as the effect of V_{BG} in the PNG regime is mostly to change the location of the p–n interface, where reflection occurs; transparency of the p–n interface itself is not strongly affected by V_{BG}, as it is in the OPG regime.

γ_{exp} is also extracted at $V_{BG} = -10$ V, showing guiding in the OPG, PNG and OPG/PNG regimes (red crosses in Fig. 3b). Values for the 'equal-epsilon' background subtraction were extracted experimentally for the OPG regime, and the PNG and OPG/PNG values were inferred from the extracted value using particle–hole symmetry ($\Omega(\varepsilon_1, \varepsilon_1) = \Omega(-\varepsilon_1, -\varepsilon_1)$) as in Fig. 2. In the OPG regime, γ_{exp} falls roughly linearly as a function of V_{TG} from 0.18 to 0, whereas in the PNG and OPG/PNG regimes it rises from 0.01 to 0.16. For V_{TG} between ~7 V and 10 V, γ_{exp} is not defined as it does not satisfy the conditions for guiding (Fig. 2a). Numerical simulations for this value of V_{BG} are shown for the three regimes for three different amounts of disorder: 0 (black), 2 (blue) and 4 nm (purple). Here we see good agreement between γ_{exp} and γ in the OPG for 2 nm of disorder, similar to Fig. 3a. However, 2 nm of interface disorder is clearly different from the experimental data in the PNG and OPG/PNG regimes, and more disorder (4 nm) is needed to obtain agreement between experiment and simulations. This is consistent with the argument of poor screening at the p–n interface used in the PNG and OPG/PNG regimes in Fig. 2.

Transparency across a graphene p–n junction decreases with applied perpendicular magnetic field (B), as discussed theoretically in refs 15 and 29, and seen experimentally in ref. 12. The reduced transparency in the magnetic field increases guiding efficiency, as demonstrated experimentally in Fig. 4. When $R^{f2}_{ic} \gg R^f_{ii}(R^f_{ii} - R_{ii})$ (the experimentally relevant case; Supplementary Fig. S1) $\Omega_{exp} \approx R^f_{ic}$. $R^f_{ic}(V_{TG})$ at $B = 5$ T is compared to the zero-field value in Fig. 4a. At $V_{BG} = -10$ V, an increase of ~0.1 kΩ in the unipolar regime and ~1 kΩ in the bipolar regime as B is increase to 5 T is observed. The inset of Fig. 4a shows $R^f_{ic}(V_{TG}, B)$, where an enhancement in resistance is apparent for $B > 2$ T. Because the ratio R^f_{ic}(bipolar)/R^f_{ic}(unipolar) increases with B, we ascribe the enhancement in R^f_{ic} (and, by inference, an increase in Ω_{exp}) as a result of an increase in the PNG contribution to current guiding. Figure 4b shows the simulated current density with $B = 5$ T, showing an improved guiding efficiency of $\gamma = 0.50$ ($\Omega = 0.55$) from the $B = 0$ value of $\gamma = 0.24$ ($\Omega = 0.29$) (see Fig. 2d for $B = 0$ value).

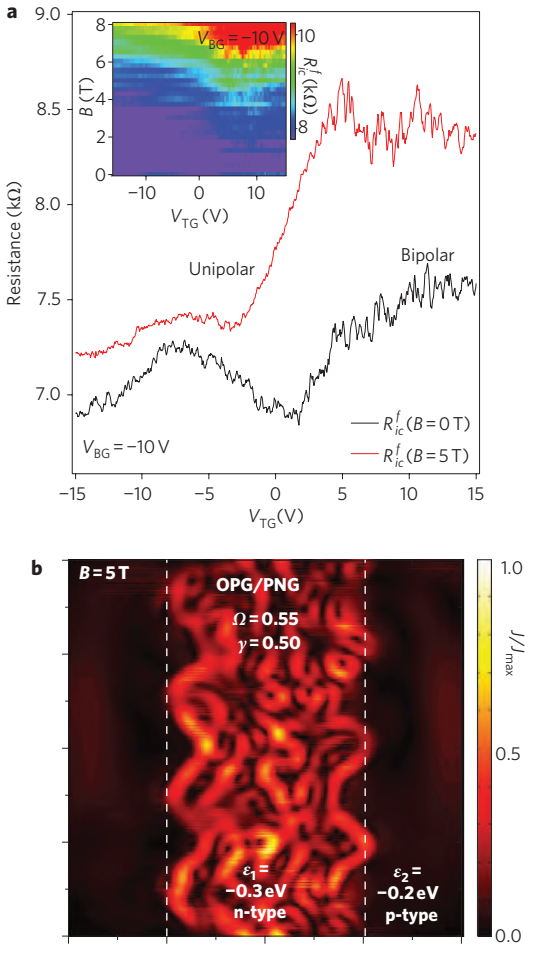

Figure 4 | Magnetic field improves gate-defined guiding. a, Inset: R^f_{ic} as a function of V_{TG} and B at $V_{BG} = -10$ V. Main panel: plot of R^f_{ic} at $B = 0$ T and $B = 5$ T. The increase in B corresponds to an increase in R^f_{ic} and the ratio R^f_{ic}(bipolar)/R^f_{ic}(unipolar), indicating a magnetic-field enhancement of the PNG contribution to R^f_{ic}. In the inset, $R^f_{ic}(V_{TG},B)$ demonstrates enhancement of R^f_{ic} for fields $B > 2$ T. **b**, Simulation of J in the OPG/PNG regime at $B = 5$ T. γ is enhanced from 0.24 (Fig. 2d) to 0.50 (Ω is enhanced from 0.29 to 0.55).

In summary, we have investigated electron guiding in graphene by tuning the carrier type and density using local electrostatic fields to create the analogue of an optical fibre. Guiding efficiency was extracted in three regimes: in the unipolar OPG regime, where the device is analogous to a fibre optic, in the bipolar PNG regime, where guiding occurs because of reflection at p–n interfaces, and the bipolar OPG/PNG regime, where both mechanisms operate. We also demonstrated experimentally that guiding efficiency increases with an applied perpendicular magnetic field, consistent with numerical results. One would expect that pseudomagnetic fields created by strain engineering[30] of greater than 300 T (ref. 31) can also enhance guiding. Improvements to guiding efficiency will result from reducing interface disorder. Engineering of a collimated source with modes within the acceptance cone of the fibre would also improve guiding. With such improvements, this approach could perhaps lead to electrically reconfigurable wiring using graphene.

Received 6 December 2010; accepted 6 January 2011; published online 13 February 2011

References

1. van Houten, H. *et al.* Coherent electron focusing with quantum point contacts in a two-dimensional electron gas. *Phys. Rev. B* **39,** 8556–8575 (1989).
2. Sivan, U., Heiblum, M., Umbach, C. P. & Strickman, H. Electrostatic electron lens in the ballistic regime. *Phys. Rev. B* **41,** 7937–7940 (1990).
3. Cheianov, V. V., Fal'ko, V. I. & Altshuler, B. L. The focusing of electron flow and a Veselago lens in graphene p–n junctions. *Science* **315,** 1252–1255 (2007).
4. Beenakker, C. W. J., Sepkhanov, R. A., Akhmerov, A. R. & Tworzydlo, J. Quantum Goos–Hänchen effect in graphene. *Phys. Rev. Lett.* **102,** 146804 (2009).
5. Zhang, F. -M., He, Y. & Chen, X. Guided modes in graphene waveguides. *Appl. Phys. Lett.* **94,** 212105 (2009).
6. Villegas, C. E. P. & Tavares, R. S. Comment on 'Guided modes in graphene waveguides' [*Appl. Phys. Lett.* 94, 212105 (2009)]. *Appl. Phys. Lett.* **96,** 186101 (2010).
7. He, Y., Zhang, F. -M. & Chen, X. Response to "Comment on 'Guided modes in graphene waveguides'" [*Appl. Phys. Lett.* 96, 186101 2010]. *Appl. Phys. Lett.* **96,** 186102 (2010).
8. Wu, Z. Electronic fibre in graphene. Preprint at http://arxiv.org/abs/1008.2495 (2010).
9. Castro Neto, A. H. *et al.* The electronic properties of graphene. *Rev. Mod. Phys.* **81,** 109–162 (2009).
10. Beenakker, C. W. J. Colloquium: Andreev reflection and Klein tunneling in graphene. *Rev. Mod. Phys.* **80,** 1337–1354 (2008).
11. Geim, A. K. Graphene: status and prospects. *Science* **324,** 1530–1534 (2009).
12. Huard, B. *et al.* Transport measurements across a tunable potential barrier in graphene. *Phys. Rev. Lett.* **98,** 236803 (2007).
13. Williams, J. R., DiCarlo, L. & Marcus, C. M. Quantum Hall effect in a gate-controlled p–n junction of graphene. *Science* **317,** 638–641 (2007).
14. Özyilmaz, B. *et al.* Electronic transport and quantum Hall effect in bipolar graphene p–n–p junctions. *Phys. Rev. Lett.* **99,** 166804 (2007).
15. Cheianov, V. V. & Fal'ko, V. I. Selective transmission of Dirac electrons and ballistic magnetoresistance of n–p junctions in graphene. *Phys. Rev. B* **74,** 041403(R) (2006).
16. Katsnelson, M. I., Novoselov, K. S. & Geim, A. K. Chiral tunnelling and the Klein paradox in graphene. *Nature Phys.* **2,** 620–625 (2006).
17. Low, T., Hong, S., Appenzeller, J., Datta, S. & Lundstrom, M. S. Conductance asymmetry of graphene p–n junction. *IEEE Trans. Electron. Dev.* **56,** 1292–1299 (2009).
18. Stander, N., Huard, B. & Goldhaber-Gordon, D. Evidence for Klein tunneling in graphene p–n junctions. *Phys. Rev. Lett.* **102,** 026807 (2009).
19. Young, A. F. & Kim, P. Quantum interference and Klein tunnelling in graphene heterojunctions. *Nature Phys.* **5,** 222–226 (2009).
20. Park, C. H., Son, Y. -W., Yang, L., Cohen, M. & Louie, S. G. Electron beam supercollimation in graphene superlattices. *Nano Lett.* **8,** 2920–2924 (2008).
21. Low, T. & Appenzeller, J. Electronic transport properties of a tilted graphene p–n junction. *Phys. Rev. B* **80,** 155406 (2009).
22. Hartmann, R. R., Robinson, N. J. & Portnoi, M. E. Smooth electron waveguides in graphene. *Phys. Rev. B* **81,** 245431 (2010).
23. Mishchenko, E. G., Shytov, A. V. & Silvestrov, P. G. Guided plasmons in graphene p–n junctions. *Phys. Rev. Lett.* **104,** 156806 (2010).
24. Cesar, E. P., Villegas, M. & Tavares, R. S. Strongly coupled modes in bi-waveguides based on graphene. *Solid State Commun.* **150,** 1350–1354 (2010).
25. Dragoman, D. & Dragoman, M. *Quantum-Classical Analogies* (Spinger, 2004).
26. Wilson, D. W., Glytsis, E. N. & Gaylord, T. K. Electron waveguiding characteristics and ballistic current capacity of semiconductor quantum slabs. *IEEE J. Quant. Electron.* **29,** 1364–1382 (1993).
27. Zhang, L. M. & Fogler, M. M. Nonlinear screening and ballistic transport in a graphene p–n junction. *Phys. Rev. Lett.* **100,** 116804 (2008).
28. Rossi, E., Bardarson, J. H., Brouwer, P. W. & Das Sarma, S. Signatures of Klein tunneling in disordered graphene p–n–p junctions. *Phys. Rev. B* **81,** 121408(R) (2010).
29. Shytov, A., Rudner, M. S. & Levitov, L. S. Klein backscattering and Fabry–Pérot interference in graphene heterojunctions. *Phys. Rev. Lett.* **101,** 156804 (2008).
30. Guinea, F., Katsnelson, M. I. & Geim, A. K. Energy gaps and a zero-field quantum Hall effect in graphene by strain engineering. *Nature Phys.* **6,** 30–33 (2009).
31. Levy, N. *et al.* Strain-induced pseudomagnetic fields greater than 300 tesla in graphene nanobubbles. *Science* **329,** 544–547 (2010).

Acknowledgements

Device fabrication was carried out using Harvard's Center for Nanoscale Systems, a member of the National Nanotechnology Infrastructure Network under National Science Foundation award ECS-0335765, and was supported in part by the Institute for Nanoelectronics Discovery and Exploration, a Nanoelectronics Research Initiative Center, and the Harvard Nanoscale Science and Engineering Center.

Author contributions

Experiments were performed by J.W. and C.M, and numerics/theory by T.L. and M.L. All authors contributed to writing the manuscript.

Additional information

The authors declare no competing financial interests. Supplementary information accompanies this paper at www.nature.com/naturenanotechnology. Reprints and permission information is available online at http://npg.nature.com/reprintsandpermissions/. Correspondence and requests for materials should be addressed to C.M.M.